LAWRENCE
LIVERMORE
NATIONAL
LABORATORY

LLNL-JRNL-401931

Source mechanisms and source parameters of March 10 and September 13, 2007, United Arab Emirates Earthquakes

Y. Al Marzooqi, K. M. Abou Elenean, A. S. Megahed, I. El-Hussain, A. Rodgers, E. Al Khatibi

March 4, 2008

Tectonophysics

Disclaimer

Source mechanisms and source parameters of March 10 and September 13, 2007, United Arab Emirates Earthquakes

Abstract

On March 10 and September 13, 2007 two felt earthquakes with moment magnitudes 3.66 and 3.94 occurred in the eastern part of United Arab Emirates (UAE). The two events were accompanied by few smaller events. Being well recorded by the digital UAE and Oman digital broadband stations, they provide us an excellent opportunity to study the tectonic process and present day stress field acting on this area. In this study, we determined the focal mechanisms of the two main shocks by two methods (polarities of P and regional waveform inversion). Our results indicate a normal faulting mechanism with slight strike slip component for the two studied events along a fault plane trending NNE-SSW in consistent a suggested fault along the extension of the faults bounded Bani Hamid area. The Seismicity distribution between two earthquake sequences reveals a noticeable gap that may be a site of a future event. The source parameters (seismic moment, moment magnitude, fault radius, stress drop and displacement across the fault) were also estimated based on the far field displacement spectra and interpreted in the context of the tectonic setting.

Keywords: United Arab Emirates; Arabian–Eurasian collision; Regional waveform inversion; Source parameters

This work performed under the auspices of the U.S. Department of Energy by Lawrence Livermore National Laboratory under Contract DE-AC52-07NA27344.

Introduction

The Arabian plate is surrounded by diverse plate boundaries. To the east and north, the Arabian Plate is colliding with the Eurasian plate along the Zagros and Bitlis sutures (Mckenzie, 1976) and presents one of the most seismically active continental regions on the Earth (Fig. 1). To the southwest and south the Arabian Plate is bounded by seafloor spreading along the Red Sea, the Gulf of Aden and the Arabian Sea. While along the northwestern side the major left lateral Dead Sea fault was located. The eastern part of Arabian Plate was affected by numerous intraplate tectonism throughout Mesozoic and Cenozoic time (Brew et al., 2001).

The Late Cretaceous Semail ophiolite is exposed in northern Oman and northeastern part of the United Arab Emirates (UAE), where it forms the world's largest exposed tract of oceanic crust and upper mantle emplaced onto continental crust (e.g. Glennie et al., 1974). High pressure rocks, including carpholite-bearing meta-sediments, garnet-blue-schists and eclogites of continental crustal origin are exposed in north-eastern Oman, structurally beneath the ophiolite (e.g. Lippard, 1983). Despite almost 100% exposure, factors including variable and complex stratigraphy, multiple episodes of deformation and rough, often inaccessible terrane have complicated the geological interpretation of the region. This has led to numerous tectonic models and much debate about the evolution of the Arabian margin in general and the high pressure terrane in particular (e.g. Searle et al., 1994, 2004; Gregory et al., 1998; Gray et al., 2000; El-Shazly et al., 2001; Breton et al., 2004; Warren and Miller, 2007). Most structural and tectonic models proposed for the emplacement of the ophiolite and underlying thrust sheets have involved the NE-directed subduction away from the passive continental margin of the Arabian plate (e.g. Le Métour et al., 1990; Hanna, 1990; Searle et al., 1994).

Following erosion and subsidence of the obducted mass, a period of quiet shallow water carbonate shelf deposition prevailed during the Eocene (Alsharhan and Nairn, 1997). A second compressional event affected the northeastern and northern margin of the Arabian Plate in the Oligocene–Miocene as a result of the final closure of the main tract of Neo-Tethys (Glennie et al., 1973). This event continues to the present day as a slow continent–continent collision responsible for the vast Alpine–

Himalayan ranges of which the Zagros Mountains are one part (Sengör, 1987). The Alpine event produced the SW-verging thrusts of the Zagros and west-verging thrusts and associated huge N–S trending folds in the Tertiary limestone cover rocks in the Emirates and northern Oman (Searle, 1985; Warrak, 1996).

Unfortunately little research has been conducted in the northern Oman Mountains on neotectonics, and there are no detailed field surveys of the Tertiary faults or assessment of their seismicity. These fault structures include the Dibba Line (Glennie et al., 1990) and the Wadi Shimal and Wadi Ham Faults (Gnos and Nicolas, 1996). These and associated faults lie within the Dibba–Masafi–Fujairah area of the northern UAE (Figs. 2, 3).

The local seismic activity of UAE is low. Historically there is no report or indication of any destructive earthquake in the country that could be a function the catalogue completeness length with respect to magnitude 5 earthquakes, combined with a potentially long recurrence interval. On March 11, 2002 a moderate (M_w ~5) earthquake occurred in Masafi area and recorded by the worldwide seismic networks. The event was felt throughout the northern emirates and was accompanied by smaller (felt) events before and after the March 11 main shock. A report on this events and accompanying damage is provided by (Othman, 2002). Rodgers et al., (2005) studied the source mechanism of Masafi 2002 event and report a normal mechanism with a slight right-lateral strike-slip component consistent with the large-scale tectonics. The focal mechanism provides for northeast trending steeply southeast-dipping normal faults similarly in orientation to an important pair of faults bounded Bani Hamid metamorphic rocks that coalesce northwards and continue north-east wards through the Khor Fakkan ophiolite block (Musson et al., 2006 & Gnos and Nicolas, 1996). Since 2003, Earthquake Monitoring Center (EMC) of Oman published yearly bulletin of earthquakes in the region. Information gathered from EMC bulletin for local earthquakes in UAE shows that there is a seismic activity in the northeastern part of UAE (Al Khatibi et al., 2007). This activity was scattered due to location errors as a result of the limited azimuth cover of Oman stations. By June, 2006 Dubai Municipality installed four broadband stations in Dubai Emirate, UAE. Dubai and Oman local seismic networks are exchanging real-time data which increase the detectability and accuracy of earthquake locations on the region. The observed

seismic activity by these two networks from June 2006 to February, 2008 indicates a clustering of activity in the northern part of UAE along Masafi-Bani Hamid area and near Wadi Nazwa gas filed.

On March 10 and September 13, 2007 two felt earthquakes occurred to the northeastern part of UAE to the northeast of Masafi 2002 earthquake (Fig. 3). The estimated average local magnitudes from the Dubai local network were 4.0 and 4.4 for the two events, respectively. The maximum observed intensity for the two events ranges from III-IV MM. The shaking was strong enough to encourage some residents to exit their houses. No body was injured on both events but the majority of Dubai peoples got frightened. The sedimentary cover dominating the major part of UAE amplifies the ground motion up to three or more times the true ones and exaggerates their affect.

UAE has witnessed rapid and flourishing economic development and long period of high rise constructions in the last few years and the majority of population occupy the flat land that covered by sedimentary cover. The biggest factor in terms of seismic hazard is believed to be the occurrences of moderate size earthquakes at shorter distances (i.e. Masafi earthquake) rather than large earthquakes that are occurred along Zagros belt (South west Iran).

In this article, we present analysis of regional waveforms recorded by Dubai and Oman local networks to estimate the source mechanisms, focal depths and source parameters of March 10, September 13, 2007 felt UAE earthquakes. The source mechanism and source parameters are useful for hazard evaluation on UAE which has now a major investment.

Location and polarities focal mechanisms

The two studied events were located using picks from the Dubai, Oman and Iran seismic networks using the HYPOCENTER location algorithm (Lienert et al., 1988). The digital waveform data were band-limited between 0.8 Hz to 20 Hz before arrival times were picked. In total, 23 and 17 crustal phases from all stations within maximum epicentral distances of 1000 km were used in this location, respectively. The closest station was ~50 km from their epicenters, and the greatest azimuthal gaps in station coverage were 126° and 180°, respectively. The location parameters are listed in Table 1. The 1-D velocity model Table 2 is used in both location and focal mechanism analysis. The RMS errors in the hypocentral estimate for the studied

events were 0.6 sec and 0.4 sec, respectively. The two events were located on Khor Fakkan block along the suggested fault branching to northeast from Wadi Ham fault and bounded Bani Hamid rocks and extends northeast (Fig. 3). The two studied events were followed by few aftershocks that do not clarify any fault geometry due to the limited number of seismic stations, high noise level and large azimuth cover.

Even though, with these location uncertainties, the integration of the whole activity located by Dubai and Oman networks constitute a nearly NE-SW trends starts north of Bulaydah-Bani Hamid towards northeast and probably extends offshore in the Arabian Gulf (Fig. 3). The Seismicity distribution along this suggested trend shows a noticeable gap that may be a site of a future event. The increase of activity on February, 2008 (10 events with local magnitudes ranges from 2.3 to 3.8) should noted worthy.

Polarities of first arriving P-waves compiled for 10 and 12 local stations were used to determine the focal mechanism for the studied events, respectively. A double-couple, fault plane solution was fit to the observations using FOCMEC (Snoke, 2003). The resulting solutions (Fig. 4) indicate normal faulting for both events trending NNE-SSW and NE-SW. Of the two nodal planes, our preferred fault plane is the NNE-SSW south-easterly dipping and consistent surface faults and large-scale tectonics. The fault parameters of the focal mechanism based on polarities solution are listed in Table 3.

Regional Waveform Inversion

Because of the source region is of a relatively low seismicity, the majority of earthquakes recorded by local and regional seismic networks along northeastern UAE are too small to be included in the Harvard CMT. Due to their frequent occurrences, these small earthquakes are particularly important for characterizing regional tectonics and constraining stress orientation. Focal mechanisms based on P-wave polarities only are insufficient to obtain well controlled focal mechanism due to the lack of appropriate crustal structure, well azimuth coverage and optimum focal depth, so they should be combined with regional waveform inversion.

The two studied events are recoded by the broadband seismographic stations in UAE and Oman. Five broadband (three-component) stations (Fig. 2) in the distance range from 50 to 107 km are used to determine the focal mechanism and focal depth. Choice of the records is mainly based on clarity of the records (signal to noise spectral ratios ≥9). Instrumental responses are removed and the two horizontal components, NS and EW, are converted to R (radial) and T (transverse). The Arabian Platform 1-D crustal model (Rodgers et al., 1999, Table 2) is used. The quality factor Q is assigned according to Swanger's law "Qs = Vs/10" where Vs is the shear velocity in m/s and QP ≈9/4 Qs (Mancilla 2001).

Long period seismic waves recorded regionally by broadband stations can be used to extract information about the earthquake source, in particular seismic moment, focal mechanism and centroid depth. The use of seismic waves at longer periods improves the estimation of earthquake source parameters because they are relatively insensitive to the effects of lateral velocity and density heterogeneities (Ritsema and Lay, 1995).

The regional waveform inversion technique reflects good results for closer broadband stations with good signal to noise ratio (Δ < 1000 km) that avoid large lateral regional velocity and density heterogeneities (Abou Elenean and Hussein, 2007). The inversion is done in lower frequency band between 0.01 to 0.12 Hz. The matrix inversion method (e.g. Ichinose, 2006) is used to invert for the point source moment tensor using Green's functions computed for a 1-D velocity model. The 1-D velocity model may not be perfect and small time shift is required for maximum correlation between the observed and synthetics. In the matrix inversion technique, the shift is not known and becomes nonlinear model parameter which has to be inverted along with the moment tensor and optimal source depth. To account for the horizontal mislocation, the synthetics were shifted relative to the observed by changing the origin time few seconds before/after location origin time during our inversion. The inversion is done imposing a deviatoric moment tensor without isotropic component. The Green's function is computed using a fast reflectivity and frequency-wave number (*f-k*) summation technique (Zeng and Anderson, 1995). The

details of the methodology were described in Ichinose and Yuehua (2000) and Ichinose et al. (2003). The preferred solution was obtained by a simple grid search over the focal depths between 1 and 30 km with 1km step and also over the origin time between 2-sec before/after the location origin time, since the origin time trades off with focal depth. The solution that has a large percentage of variance reduction and double couple component is selected. The percentage of variance reduction is found by:

$$VR = \left[1 - \sum_i \frac{\sqrt{(data_i - synth_i)^2}}{\sqrt{data_i^2}} \right] * 100 \qquad (1)$$

Where *data* and *synth* are the data and synthetic time series respectively and the summation is performed for all stations and components. Figure (5) shows the comparison between the observed and synthetic waveforms for the preferred solution with high percentage of variance reduction and double couple component of March 10, 2007 earthquake. The optimal origin time form our inversion (14 sec) is consistent with the location origin time seconds (14.3 sec) and the fit is satisfactory that indicates the adequacy of the used 1-D model in that lower frequency band in our inversion. The focal mechanism was stable over a wide range focal depths and represent normal fault with a slight strike slip component in good agreement with the polarities solution. The focal mechanism parameters are listed in Table 3. Figure (6) illustrates the changes in percent of variance reduction and source mechanisms as a function of tested focal depths.

Figure (7) shows the comparison between the observed and synthetic waveforms for the preferred solution with high percentage of variance reduction and double couple component of September 13, 2007 earthquake. The optimal origin time seconds (7 sec) is also consistent with the location origin time seconds and the fit is satisfactory. The focal mechanism of this event was also stable over a wide range of focal depths and preferred solution indicates also shows normal fault trending NNE with a slight strike slip component. Figure (8) illustrates the changes in percent of variance reduction and source mechanisms as a function of tested focal depths while its focal mechanism parameters are listed in Table 3.

Source parameters

Source parameters are useful in micro-zonation and the assessment of seismic hazard. The seismic moment (M_o), fault radius (r_o), average displacement across the fault (d_o), stress drop ($\Delta\sigma$) and the moment magnitude (M_w) were determined for the two studied events using the P-wave far-field amplitude displacement spectra. The analyzed data consist of four broadband stations that overlie hard rock sites and have good signal to noise ratio. We apply our analysis for vertical components only and we ignore the UAE stations that overlie sedimentary cover to avoid the site effect and spectra complexity. The analyzed stations are located within epicentral distances ranges from 50 km to 135 km. First, the signal was corrected to zero baseline and the instrumental response. A cosine taper was applied to the selected signal window. Signals windows of varying length were tested in order to select a length that would avoid contamination from other phases and maintain the resolution and stability of the spectra. A selected signal windows ranges from 6 to 8 sec.

Following Brune (1970, 1971), the far field displacement spectra d(f) is:

$$d(f) = \frac{G(r,h)*D(f)*M_o*kk}{4\pi\rho v_c^3 * \sqrt{1+\left(\frac{f}{f_o}\right)^{2\gamma}}} \qquad (2)$$

where *G(r, h)* is geometrical spreading which is a function of both epicentral distance (r) and focal depth (h). *D(f)* is the diminution function due to anelastic attenuation that includes path and near surface attenuation, f is the frequency, f_o is the corner frequency and γ is the source spectral fall off. While ρ is the density, V_c is the velocity of either shear wave or compressional wave and *kk* is a factor to correct for the free surface effect and radiation pattern. In our analysis, the geometrical spreading has been defined according to Herrmann and Kijko (1983) relation. Meanwhile, the anelastic attenuation $e^{-\pi ft}/Q_c(f)$ with $Q_c(f)$ being the quality factor, t is the travel time was taken into account by a quality factor Q_P of 648 that presents the average along the path.

The attenuation of seismic wave near the site is commonly accounted for by $e^{-\pi fk}$ (Singh et al., 1982). Assuming an omega-square Brune's source model, the *k* parameter, low frequency spectral amplitude Ω_o and corner frequency f_o are estimated using the nonlinear least square inversion techniques. The estimated value of *k* parameter ranges from 0.01 to 0.03. For circular source model the seismic moment,

fault radius (r_o), displacement across the fault and the moment magnitude can be derived from the P-wave displacement spectra following Brune's (1970, 1971), Hanks and Wyss (1972) and Kanamori (1977) relations:

$$M_o = \frac{4\pi\rho v_P^3}{F * R_{\theta\phi} * G(r, h)} \quad (3)$$

$$r_o = \frac{2.34 V_P}{2\pi f_o} \quad (4)$$

$$\Delta\sigma = \frac{7 M_o}{16 r_o^3} \quad (5)$$

$$d_o = \frac{M_o}{\pi\rho V_S^2 r_o} \quad (6)$$

$$M_w = 2/3\ log_{10}(M_o) - 10.73 \quad (7)$$

where ρ, V_P and V_S are picked from Table 2 according to the source depth. F, free surface effect is estimated for individual station based on V_P/V_S and the emergence angles of P and S-wave using the focmec package (Snoke, 2003). An Average value of $R_{\theta\phi}$ of 0.52 was assumed (Boore and Boatwright, 1984). The obtained source parameters for the two studied events are listed at Tables 4, 5 whereas the fitted displacement spectra at some stations are plotted in figures 9, 10.

For each event, the average values $\langle x \rangle$ were computed for seismic moment, source radius, stress drop, average displacement and moment magnitude Table 6. Calculation was made following Archuleta et al. (1982):

$$\langle x \rangle = antilog \left(\frac{1}{N_s} \sum_{i=1}^{N_s} \log x_i \right) \quad (8)$$

where N_s is the number of stations used. This procedure gives equal weight to each observation. In the case of simple arithmetic average, the result would be biased towards larger values. Another reason is that the errors associated with Ω_o and r_o are log-normally distributed (Garcia-Garcia, 1996). The standard deviation of the logarithm, S.D.$\left[\log\langle x \rangle\right]$, and a multiplicative error factor, E_x, were calculated as:

$$E_x = antilog \left(S.D.\left[\log\langle x \rangle\right] \right) \quad (9)$$

The calculated source parameters of the first event of March 10, 2007 are relatively consistent that indicate a homogenous rupture. Meanwhile the parameters of the second event of September 13, 2007 show a slight scatter that may be related to a directivity effect of rupture towards NNE (corner frequency and stress drop are relatively larger at BAN station compared with others stations).

Discussion

Estimation of accurate hypocentral parameters and focal mechanism can provide important information about the slip, fault structure at depth and the stress field in seismically active fault zone. In this study, we used the broad band records of Dubai and Oman to obtain a precise location and focal mechanism of two felt smaller events of March 10 and September 13, 2007. The hypocenters of the two events were located on Khor Fakkan block between Wadi Shimal Fault and pair of faults branching to the northeast from the Wadi Ham Fault (Gnos and Niclos, 1996).

The focal mechanisms of two studied events determined by two methods (polarities and regional waveform inversion) indicate normal faulting mechanisms with slight strike slip component. Because the dominant surface faults crossing the area are trending NNE and south-easterly dipping, we argue the NNE plane with slight right lateral strike slip movement from our solution as the fault plane. The right-lateral strike-slip component of the mechanism is consistent with right-lateral motion along the Oman Line in Iran (e.g. Kadinsky-Cade and Barazangi, 1982, Rodgers et al., 2005). The Oman Line defines the boundary between continental collision of the Arabian and Eurasian Plates along the Zagros Thrust and oceanic-continental convergence in the Makkran region. Convergence along the Zagros Thrust is much faster than along the Makkran, leading to dextral motion along the Zendan Fault Zone (see Fig. 2, inset). Our solutions are in good agreement with the solutions of March 11, 2002 Masafi (Rodgers et al., 2005, Fig. 3). The normal component is dominant and is consistent with brittle extension of the Khor Fakkan Block, a massif of mainly Semail peridotite bounded to the west and northwest by the Wadi Shimal Fault, and bounded to the southwest by the Wadi Ham Fault (Rodgers et al., 2005). Searle and Cox (1999) represent the two northeast trending faults at Bulaydah as reverse faults. Meanwhile, Searle (1988), Boote et al. (1990) and Rodgers et al. (2005) suggested a

reactivation of the NNE reverse faults as normal faulting in the present day stress field.

Harvard CMT solutions for larger earthquakes (Mw ≥ 6, Fig.1) to the north of UAE along Zagros Belt show a dominant NNW to NW thrust faults with right-lateral strike slip component. The P-axis of these solutions generally trends ~NNE. In the present stress field, where the maximum horizontal stress is oriented ~NNE, roughly parallel faults will be essentially normal, whereas roughly perpendicular ones is thrust faults. Other faults in intermediate directions will entail predominant strike-slip movements.

Conclusions

Focal mechanism of two felt occurred on March 10, September 13, 2007 using polarities and regional waveform inversion techniques indicate a normal faulting mechanism with slight right-lateral strike-slip component. The normal faulting mechanism is consistent with relaxation of the Khor Fakkan Block as well as with a slight right-lateral strike-slip component along Oman line. The event provides some constraint on active tectonics in the relatively aseismic northern UAE and Oman Mountains.

The seismic activity revealed by Dubai and Oman networks constitute a nearly NE-SW trends starts north of Bulaydah-Bani Hamid towards north-east and probably extends offshore in the Arabian Gulf and shows a noticeable gap that may be a site of a future event. The increase of activity on February, 2008 (10 events with local magnitudes ranges from 2.3 to 3.8) should noted worthy.

The seismic moment and moment magnitude of March 10 earthquake based on the regional waveform inversion are 3.79×10^{21} dyne.cm and 3.66 which are nearly similar to the values derived from the displacement spectra 3.92×10^{21} dyne.cm and 3.67, respectively. The estimated fault length, displacement across the fault and stress drop based on displacement spectra are 739 m, 0.67 cm and 4.19 bar, respectively.

Meanwhile, the seismic moment and moment magnitude of September 13 earthquake based on the regional waveform inversion are 9.98×10^{21} dyne.cm and 3.94 which have good agreement with the values derived from the displacement spectra

$10.73x10^{21}$ dyne.cm and 3.95, respectively. The estimated fault length, displacement across the fault and stress drop for this event are 827 m, 1.48 cm and 8.28 bar, respectively.

Our stress drop values for the studied events are smaller than usual values of type III intraplate earthquakes (midplate) but similar to II (intraplate, plate boundary related) type of Schloz (1990). This observation may be related to the tectonic situation of UAE and Oman closer to the major Arabian-Eurasian plate boundary that might reactivate previous weakness zones. These earthquakes caused considerable alarm in the northern Emirates and highlight the fact that damaging earthquakes can occur in this region.

References

Abou Elenean, K. M. and Hussein, H. M., 2007: Source mechanism and source parameters of May 28, 1998 earthquake, Egypt. J. Seismol., 11, 259-274.

Al Khatibi, E., Al Marzooqi, Y., Megahed, A., Mathias, F. and Mallalah, A., 2007. Preliminary Seismicity Of United Arab Emirates Deduced From Dubai Seismic Network, unpublished.

Alsharhan, A.S., Nairn, A.E.M., 1997. Sedimentary Basins and Petroleum Geology of the Middle East. Elsevier Science, Amsterdam. 940 pp.

Archuleta, R.J., E. Cranswinck, CH. Mueller and P. Spudich, 1982. Source parameters of the 1980 Mammoth lakes, California, earthquakes sequence, J. Geophys. Res., **87**, 4595-4607.

Boore, D.M. and Boatwright, J., 1984. Average body-wave radiation coefficients. Bull Seismol. Soc. Am., 74(5):1615-1621.

Boote, D.R.D., Mou, D., Waite, R.I., 1990. Structural evolution of the Suneinah Foreland, central Oman Mountains. In: Robertson, A.H.F., Searle, M.P., Ries, A.C. (Eds.), The Geology and Tectonics of the Oman Region, Geological Society Special Publication vol. 49, pp. 397– 418.

Breton, J.P., Béchennec, F., Le Métour, J., Moen-Maurel, L., Razin, P., 2004. Eoalpine (Cretaceous) evolution of the Oman Tethyan continental margin: insights from a structural field study in Jebel Akhdar, Oman Mountains. GeoArabia 9, 41-58.

Brune, J. N., 1970. Tectonic stress and the spectra of seismic shear waves from earthquakes. J. Geophys. Res., 75, pp. 4997-5009.

Brune, J. N., 1971. Correction. J. Geophys. Res., 76. 5002.

El-Shazly, A.K., Brocker, M., Hacker, B., Calvert, A., 2001. Formation and exhumation of blueschists and eclogites from NE Oman: new perspectives from RbeSr and 40Ar/39Ar dating. Journal of Metamorphic Geology 19, 233-248.

Garcia-Garcia, J.M., Vidal, F., Romacho, M.D., Martin-Marfil, J.M., Posadas, A. and Luzon, F., 1996. Seismic source parameters for microearthquakes of the Granada basin (southern Spain), Tectonophysics, 261, 51-66.

Glennie, K.W., Boeuf, M.G., Hughes-Clarke, M.H.W., Moody-Stuart, M., Pilaar, W.F., Reinhardt, B.M., 1974. Geology of the Oman Mountains. In: Verhandelingen Koninklijk Nederlands Geologisch Mijnbouwkundidg Genootschap Transactions, 31. 423.

Glennie, K.W., Boeuf, M.G.A., Hughes Clarke, M.W., Moody-Stuart, M., Pilaar, W.F.H., Reinhardt, B.M., 1973. Late Cretaceous nappes in Oman Mountains and their geologic evolution. Bull. Am. Assoc. Pet. Geol. 57, 5 – 27.

Glennie, K.W., Hughes Clarke, M.W., Boeuf, M.G.A., Pilaar, W.F.H., Reinhardt, B.M., 1990. Inter-relationship of Makran–Oman Mountains belts of convergence. In: Robertson, A.H.F., Searle, M.P., Ries, A.C. (Eds.), The Geology and Tectonics of the Oman Region, Geological Society Special Publication, vol. 49, pp. 773– 786.

Gnos, E., Nicolas, A., 1996. Structural evolution of the northern end of the Oman Ophiolite and enclosed granulites. Tectonophysics 254, 111 – 137.

Gray, D.R., Gregory, R.T., Miller, J.M., 2000. A new structural profile along the Muscat-Ibra transect, Oman: Implications for emplacement of the Samail ophiolite. In: Dilek, Y., Moores, E.M., Elthon, D., Nicholas, A. (Eds.), Ophiolites and Oceanic Crust: New Insights from Field Studies and the Ocean Drilling Programme. Geological Society, America, Special Paper, vol. 349. Boulder, Co, pp. 513-523.

Gregory, R.T., Gray, D.R., Miller, J.M., 1998. Tectonics of the Arabian margin associated with the formation and exhumation of high-pressure rocks, Sultanate of Oman. Tectonics 17 (5), 657-670.

Hanks, T.C. and M. Wyss, 1972. The use of body-wave spectra in the determination of seismic-source parameters, Bull. Seismol. Soc. Am., 62, 561-589.

Hanna, S., 1990. The alpine deformation of the Central Oman mountains. In: Robertson, A.F.H., Searle, M.P., Ries, A.C. (Eds.), The Geology and Tectonics of the Oman Region. Geological Society, London, Special Publication 49, pp. 341–359.

Herrmann, R. and A. Kijko, 1983. Modelling some empirical vertical component Lg relations, Bull. Seism. Soc. Am. 73,157-171.

Ichinose, G. and Yuehua, Z., 2000: Waveform modeling and moment tensor inversion tools, http://www.seismo.unr.edu/htdocs/students/Ichinose/WaveformTools.

Ichinose, G., 2006. Moment tensor inversion Toolkit (MTINV) version 0.9, released November, 2006, http://www.seismo.unr.edu/htdocs/students/Ichinose/

Ichinose, G., Anderson, J., Smith, K. and Yuehua, Z., 2003: Source parameters of Eastern California and Western Nevada Earthquake from regional moment tensor inversion. Bull. Seism. Soc. Am. 93, 61-84.

Kadinsky-Cade, K., Barazangi, M., 1982. Seismotectonics of southern Iran: the Oman line. Tectonics 1, 389– 412.

Kanamori, H., 1977. The energy release in great earthquakes. Journal of Geophysical Research, 82, 1981-1987.

Le Métour, J., Rabu, D., Tegyey, M., Bechennec, F., Beurrier, M., Villey, M., 1990. Subduction and obduction: two stages in the Eo-Alpine tectonometamorphic evolution of the Oman mountains, In: Robertson, A.F.H., Searle, M.P., Ries, A.C. (Eds.), The Geology and Tectonics of the Oman Region. Geological Society of London Special Publication 49, pp. 327–339.

Lienert, B., Berg, E., Frazer, L., 1988. HYPOCENTER, an earthquake location method using centered, scaled and adaptively least squares. Bull. Seismol. Soc. Am. 76, 771–783.

Lippard, S.J., 1983. Cretaceous high pressure metamorphism in NE Oman and its relationship to subduction and ophiolite nappe emplacement. Journal of the Geological Society London, 140, 97-104.

Mancilla, P., 2001: Surface wave dispersion about the New Madrid Region, M. Sc. Thesis, Faculty of the Graduate School of Saint Louis University, USA.

Musson, R.W., Northmore, K.J., Sargeant, S.L., Phillips, E.R., Boon, D. Long, D., McCue, K. and Ambraseys, N.N., 2006: The geology and geophysics of the United Arab Emirates, Volume 4: Geological Hazards, Published by the Ministry of Energy, UAE, pages: 239.

Ritsema, J. and Lay, T., 1995: Long period regional waves moment tensor inversion for earthquakes in the western United States, J. Geophys. Res., 100, 9853-9864.

Rodgers, A., Fowler,A., Al-Amri, A. and Al-Enezi, A., 2005. The March 11, 2002 Masafi, United Arab Emirates earthquake:Insights into the seismotectonics of the northern Oman Mountains. Teconophysics 415, 57-64.

Rodgers, A., Walter, W., Mellors, R., Al-Amri, A., Zhang, Y., 1999: Lithospheric structure of the Arabian Shield and Platform from complete regional waveform modeling and surface wave group velocities, Geophys. J. Int. 138, 871– 878.

Scholz, C. H., 1990. The mechanics of earthquake faulting, Cambridge University Press, p. 326-329.

Searle, M., Cox, J., 1999. Tectonic setting, origin and obduction of the Oman ophiolite. Bull. Geol. Soc. Am. 111, 104– 122.

Searle, M.P., 1985. Sequence of thrusting and the origin of culminations in the northern and central Oman Mountains. J. Struct. Geol. 7, 129–143.

Searle, M.P., 1988. Thrust tectonics of the Dibba zone and the structural evolution of the Arabian continental margin along the Musandam Mountains (Oman and United Arab Emirates). J. Geol. Soc. Lond. 145, 43– 53.

Searle, M.P., Warren, C.J., Parrish, R.R., Waters, D.J., 2004. Structural evolution, metamorphism and restoration of the Arabian continental margin, Saih Hatat region, Oman Mountains. Journal of Structural Geology 26, 451-473.

Searle, M.P., Waters, D.J., Martin, H.N., Rex, D.C., 1994. Structure and metamorphism of blueschist-eclogite facies rocks from the northeastern Oman mountains. Journal of the Geological Society London 151, 555-576.

Sengör, A.M.C., 1987. Tectonics of the Tethy sides: orogenic collage development in a collisional setting. Annu. Rev. Earth Planet. Sci. 15, 213–244.

Singh, S.K., Apsel R.J., Fried, J. and Brune, J.N., 1982. Spectral attenuation of SH-waves along the Imperial fault. Bulletin of the Seismological Society of America. 72, 2003-2016.

Snoke, A., 2003: Focal mechanism determination software (FOCMEC package), http://www.geol.vt.edu/outreach/vtso/focmec

Warrak, M., 1996. Origin of the Hafit structure: implications for timing the Tertiary deformation in the northern Oman Mountains. J. Struct. Geol. 18, 803– 818.

Warren. C. J., Miller, J. Mcl., 2007. Structural and stratigraphic controls on the origin and tectonic history of a subducted continental margin, Oman Journal of Structural Geology 29, 541-558.

Zeng, Y. and Anderson, J., 1995: A method for direct computation of the differential seismogram with respect to the velocity change in a layered elastic solid, Bull. Seismol. Soc. Am., 85, 300-307.

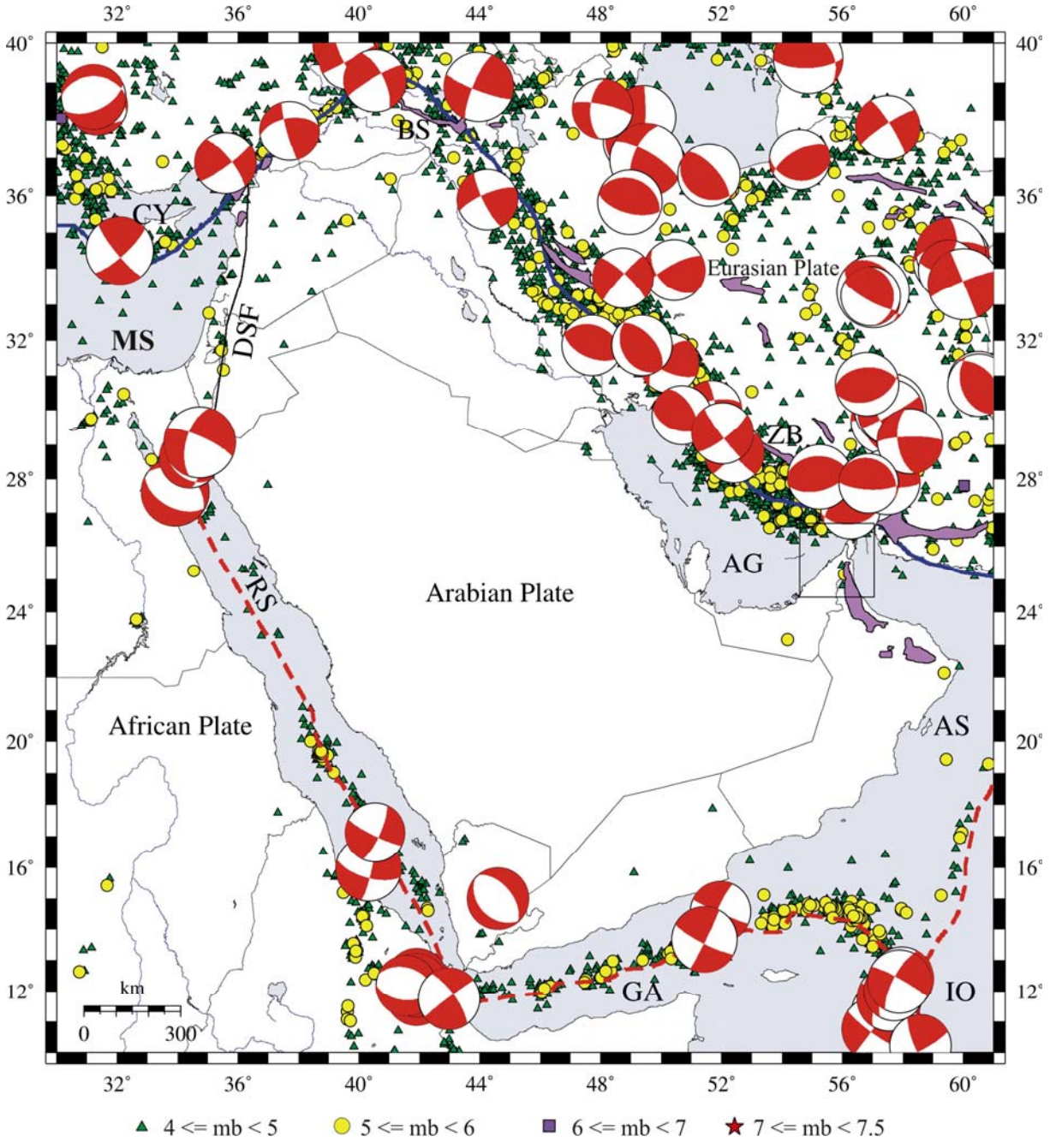
32°
36°
40°
44°
48°
52°
56°
60°
40°
36°
32°
28°
24°
20°
16°
12°
BS
CY
MS
DSF
Eurasian Plate
ZB
AG
RS
Arabian Plate
African Plate
AS
GA
IO
km
0
300
4 <= mb < 5
5 <= mb < 6
6 <= mb < 7
7 <= mb < 7.5

Fig. 1

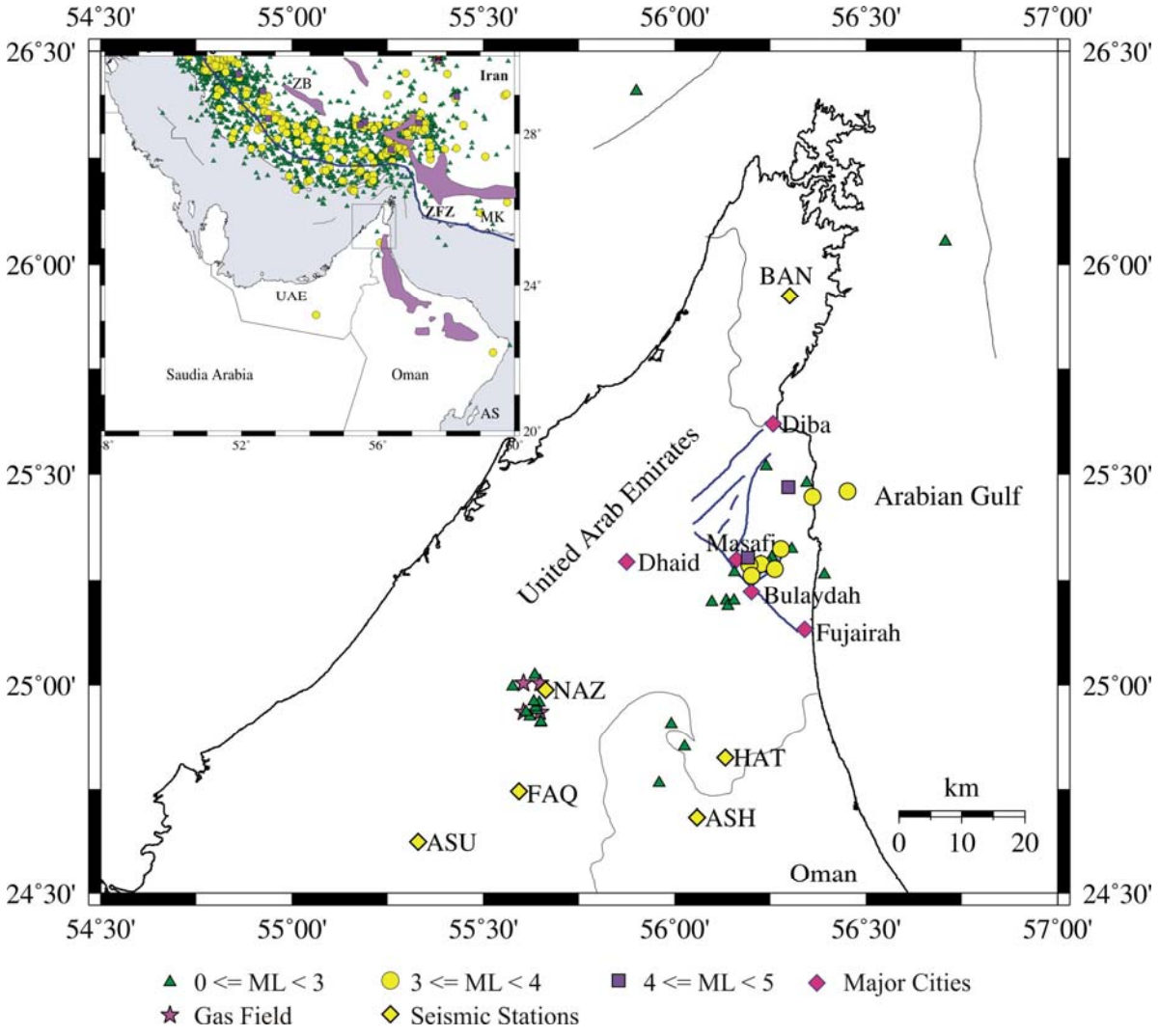
54°30'
55°00'
55°30'
56°00'
56°30'
57°00'
26°30'
26°00'
25°30'
25°00'
24°30'
Iran
ZB
ZFZ
MK
UAE
Saudia Arabia
Oman
AS
28°
24°
20°
52°
56°
BAN
Diba
Arabian Gulf
United Arab Emirates
Masafi
Dhaid
Bulaydah
Fujairah
NAZ
HAT
FAQ
ASH
ASU
Oman
km
0 10 20
0 <= ML < 3
3 <= ML < 4
4 <= ML < 5
Major Cities
Gas Field
Seismic Stations

Fig. 2

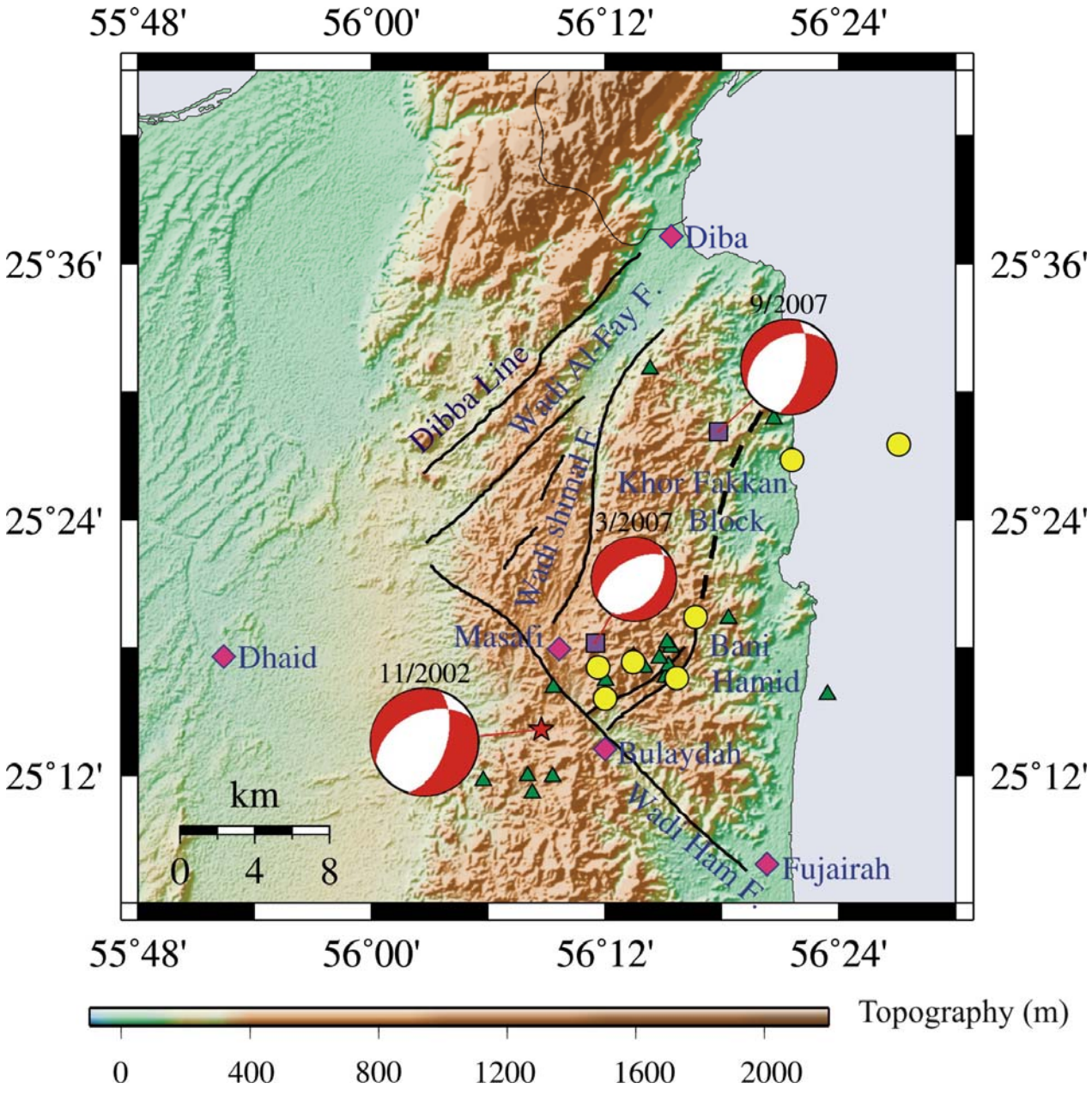
55°48'
56°00'
56°12'
56°24'
25°36'
25°24'
25°12'
Diba
9/2007
Dibba Line
Wadi Al-Fay F.
Wadi shimal F.
Khor Fakkan
Block
3/2007
Masafi
Bani
Hamid
Dhaid
11/2002
Bulaydah
Wadi Ham F.
Fujairah
km
0 4 8
Topography (m)
0 400 800 1200 1600 2000

Fig. 3

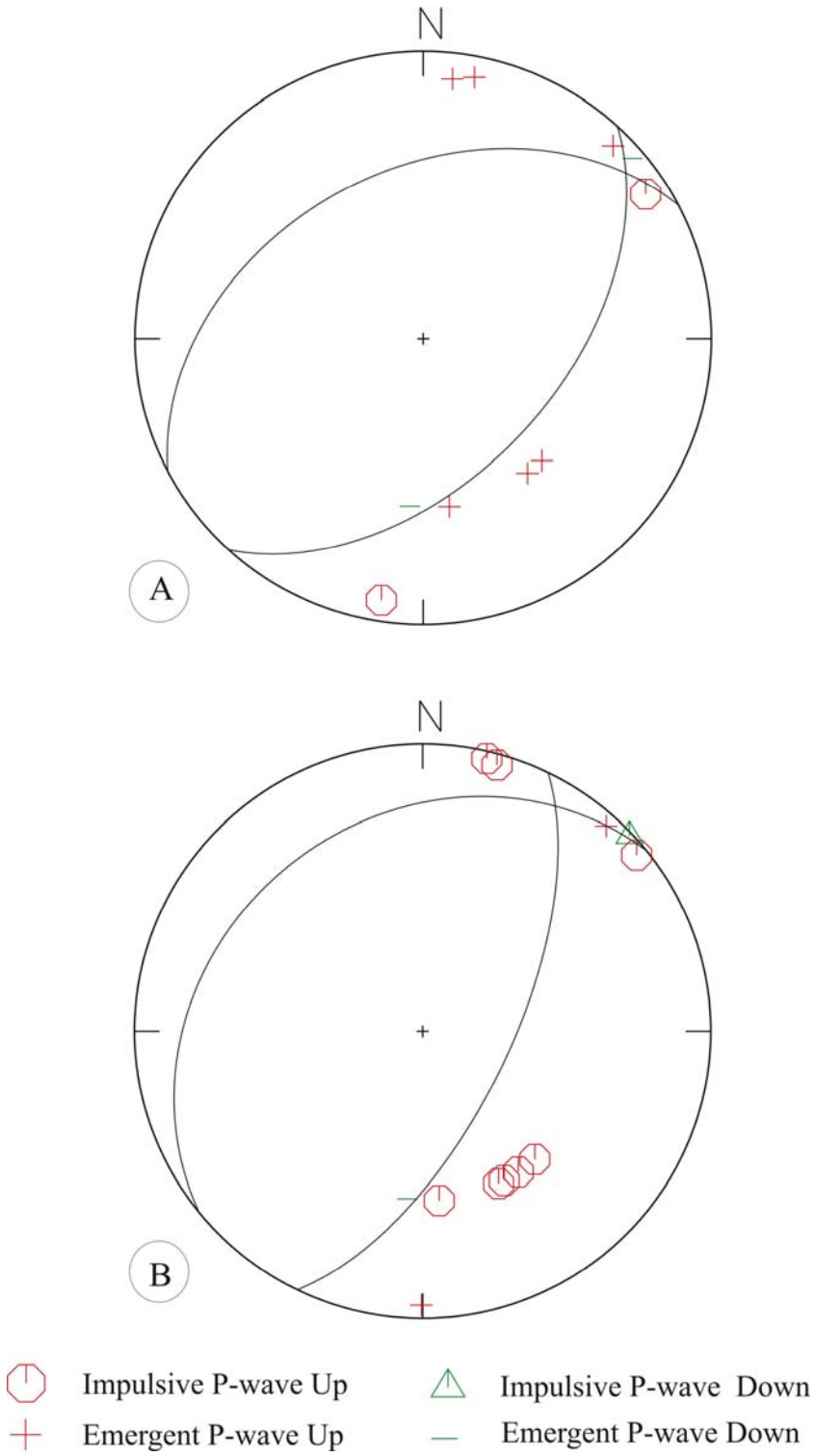
N
A
N
B
Impulsive P-wave Up
Impulsive P-wave Down
Emergent P-wave Up
Emergent P-wave Down

Fig. 4

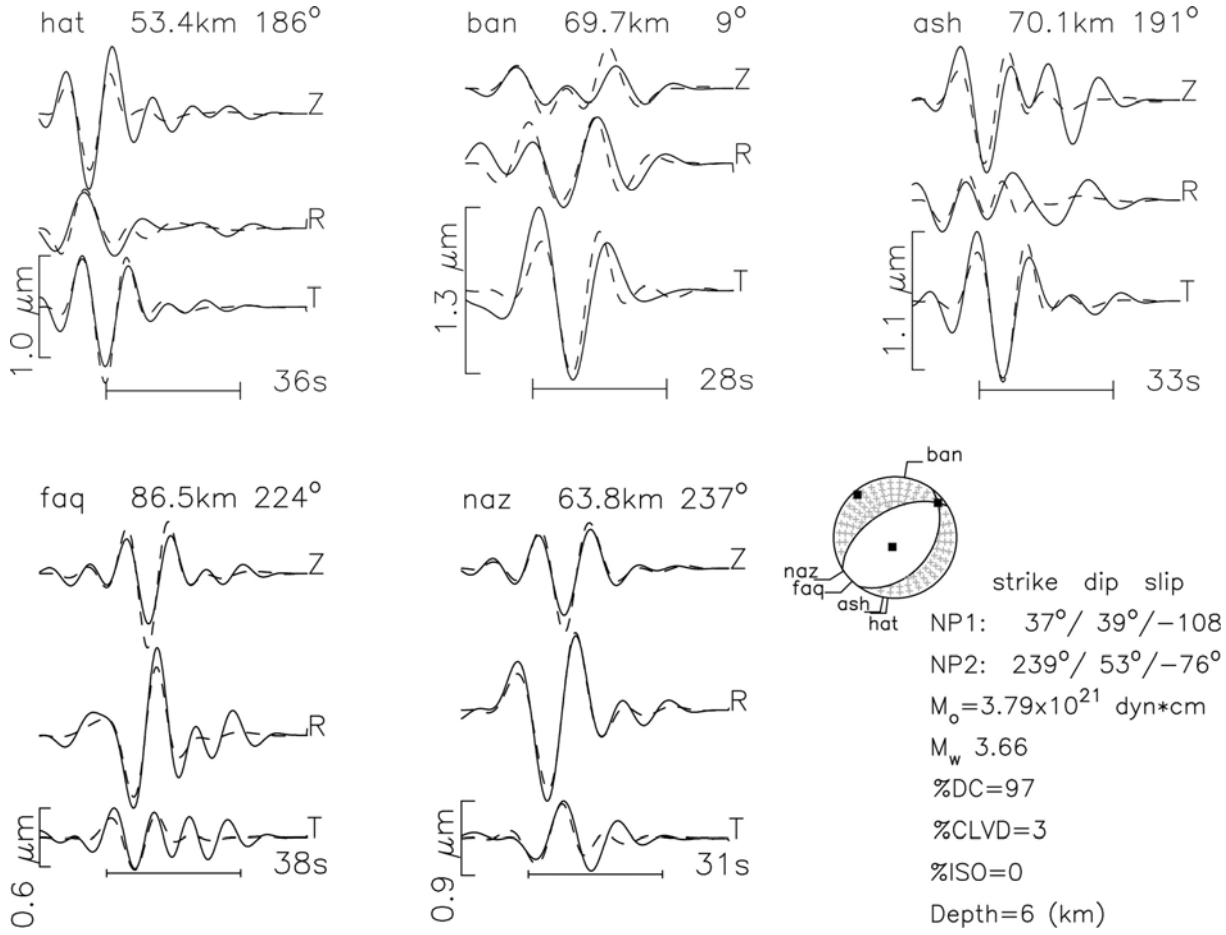
hat 53.4km 186°
Z
R
T
1.0 μm
36s
ban 69.7km 9°
Z
R
T
1.3 μm
28s
ash 70.1km 191°
Z
R
T
1.1 μm
33s
faq 86.5km 224°
Z
R
T
0.6 μm
38s
naz 63.8km 237°
Z
R
T
0.9 μm
31s
ban
naz
faq
ash
hat
strike dip slip
NP1: 37°/ 39°/−108
NP2: 239°/ 53°/−76°
M$_o$=3.79x10^{21} dyn*cm
M$_w$ 3.66
%DC=97
%CLVD=3
%ISO=0
Depth=6 (km)

Fig. 5

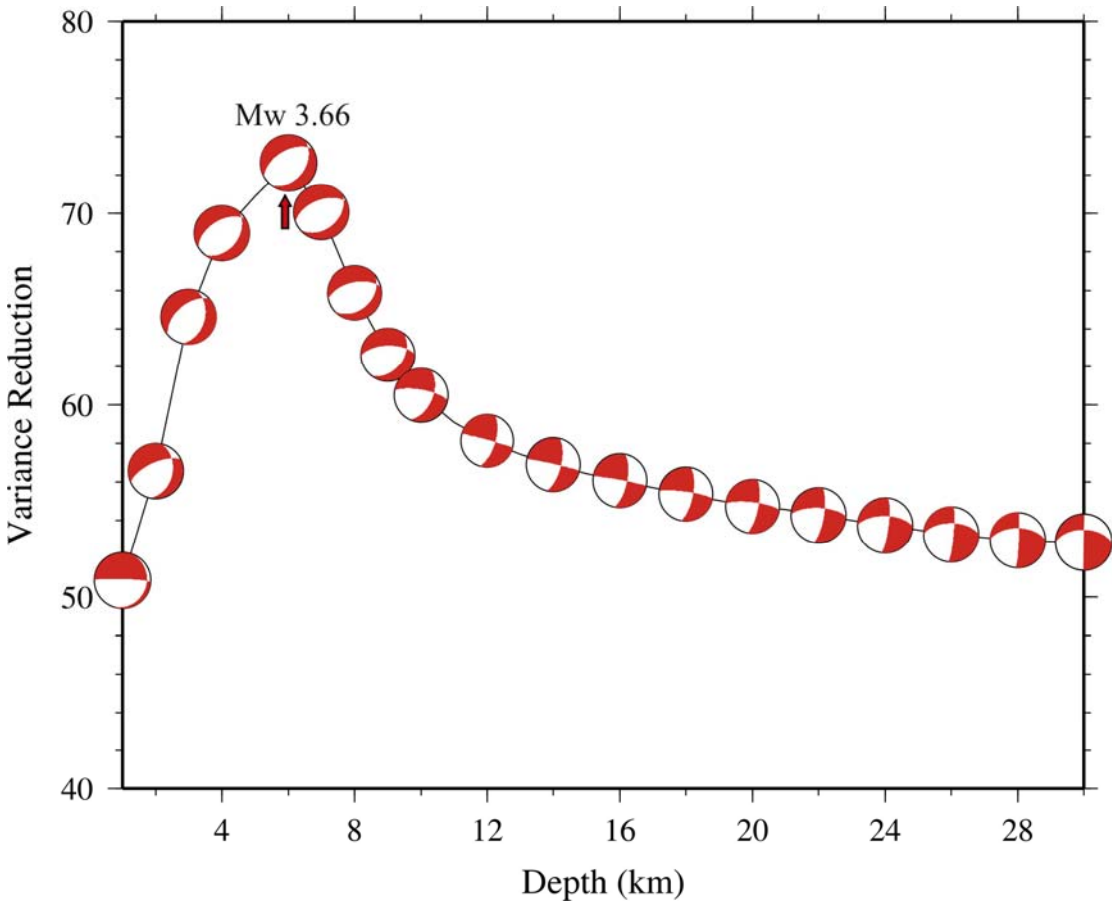
Mw 3.66
Variance Reduction
80
70
60
50
40
4
8
12
16
20
24
28
Depth (km)

Fig. 6

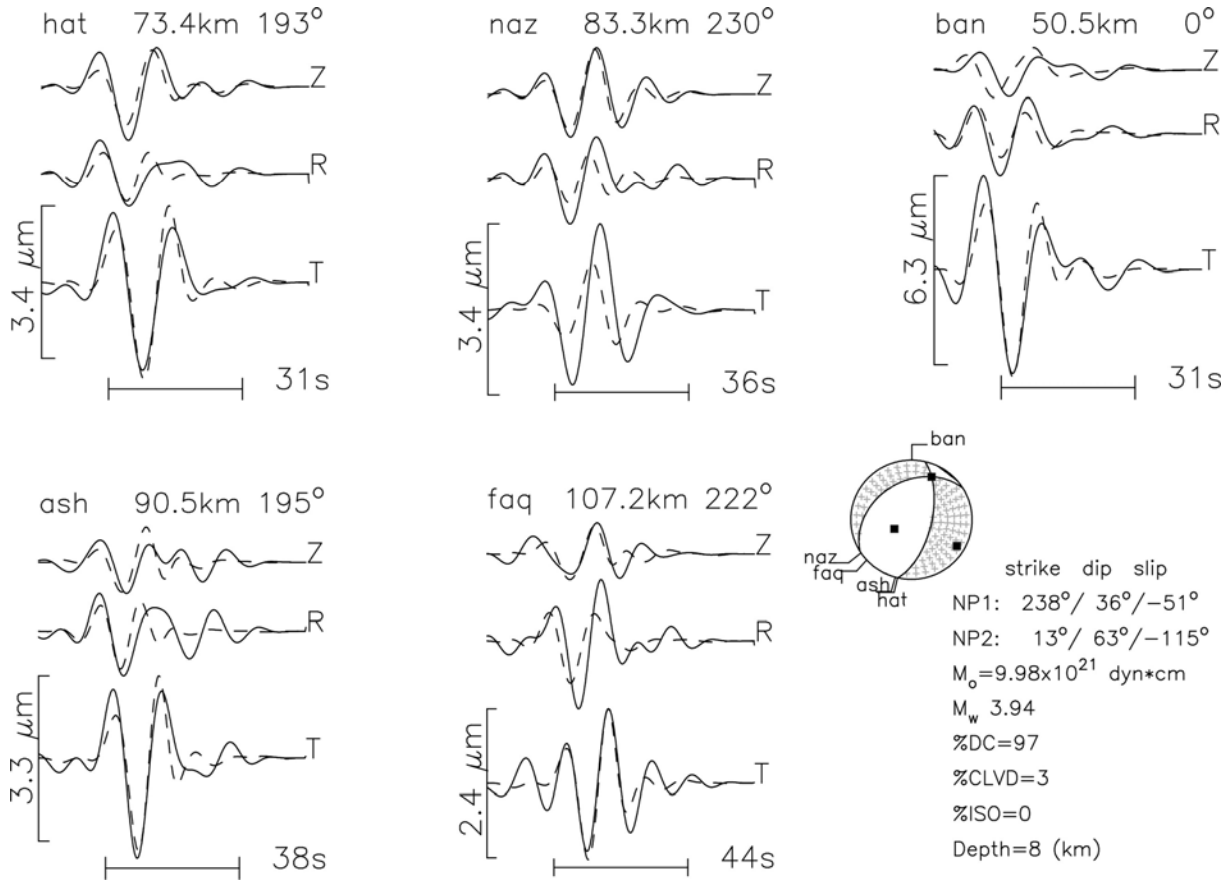
hat 73.4km 193°
Z
R
T
3.4 μm
31s
naz 83.3km 230°
Z
R
T
3.4 μm
36s
ban 50.5km 0°
Z
R
T
6.3 μm
31s
ash 90.5km 195°
Z
R
T
3.3 μm
38s
faq 107.2km 222°
Z
R
T
2.4 μm
44s
ban
naz
faq
ash
hat
strike dip slip
NP1: 238°/ 36°/−51°
NP2: 13°/ 63°/−115°
M0=9.98x10^21 dyn*cm
Mw 3.94
%DC=97
%CLVD=3
%ISO=0
Depth=8 (km)

Fig. 7

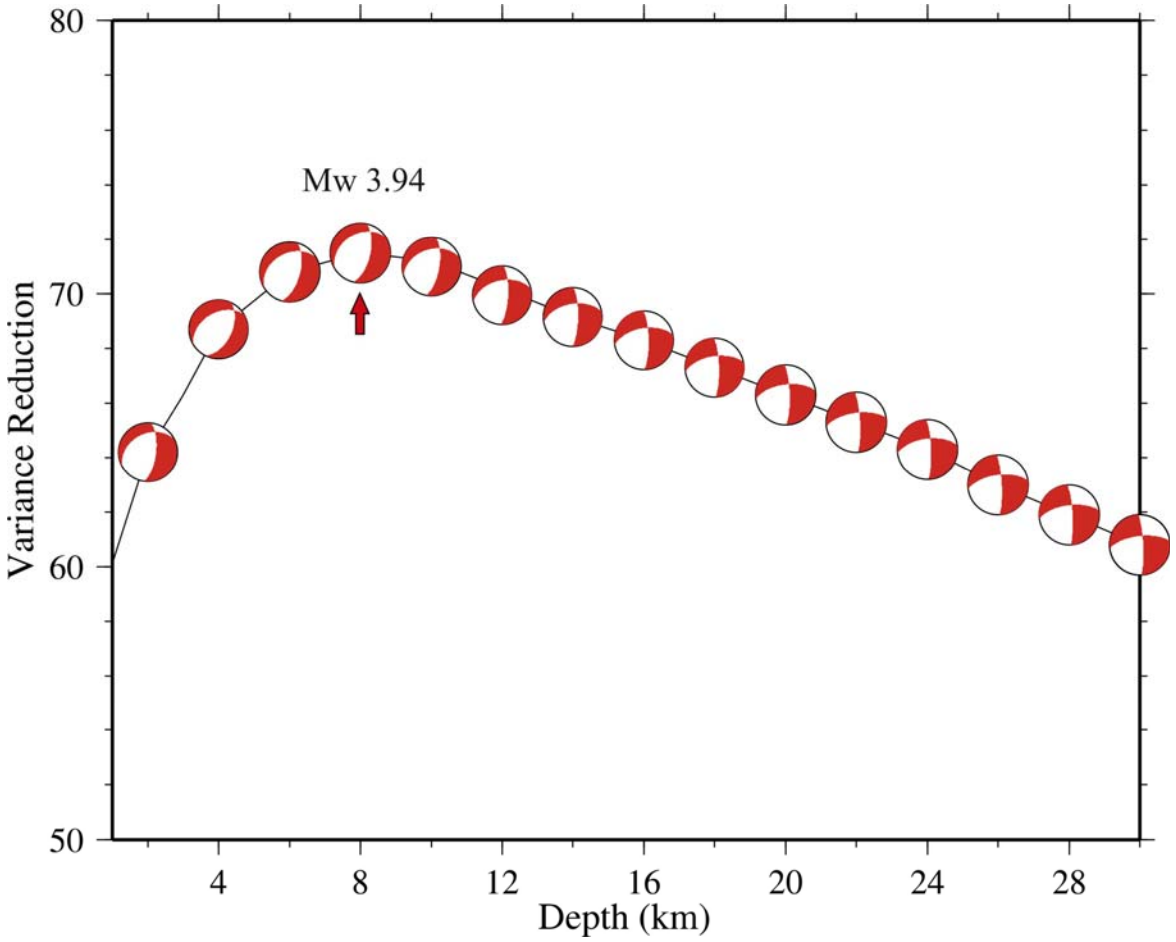

Fig. 8

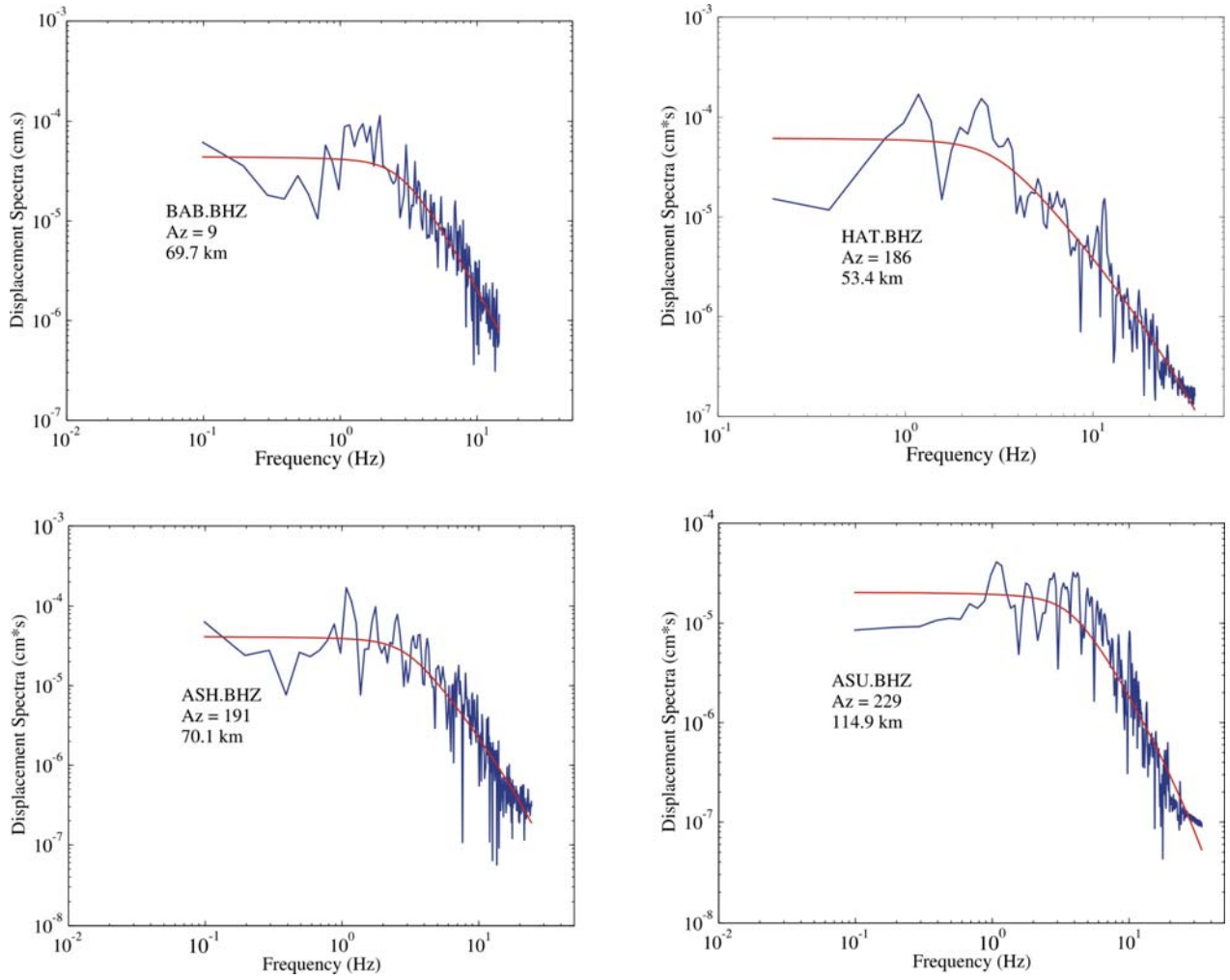
Displacement Spectra (cm.s)
BAB.BHZ
Az = 9
69.7 km
Frequency (Hz)
Displacement Spectra (cm*s)
HAT.BHZ
Az = 186
53.4 km
Frequency (Hz)
Displacement Spectra (cm*s)
ASH.BHZ
Az = 191
70.1 km
Frequency (Hz)
Displacement Spectra (cm*s)
ASU.BHZ
Az = 229
114.9 km
Frequency (Hz)

Fig. 9

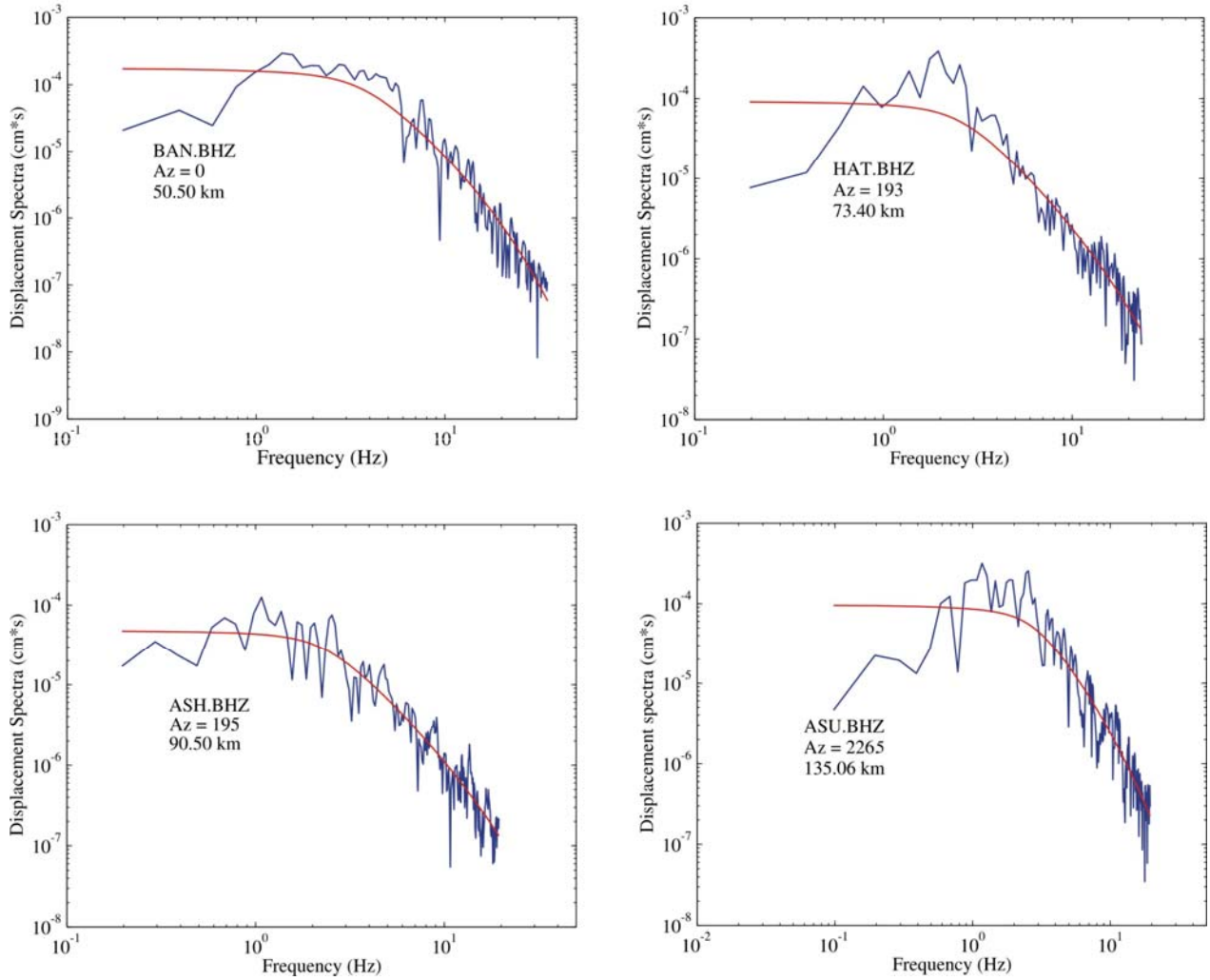
BAN.BHZ
Az = 0
50.50 km
HAT.BHZ
Az = 193
73.40 km
ASH.BHZ
Az = 195
90.50 km
ASU.BHZ
Az = 2265
135.06 km
Displacement Spectra (cm*s)
Displacement spectra (cm*s)
Frequency (Hz)

Fig. 10

Figure captions

Fig. 1. Tectonic boundaries of the Arabian plate. Seismicity data was complied from ISC (1964-2005) and NEIC (2005-2007) for earthquakes with mb ≥ 4. Focal mechanisms represent Harvard CMT solutions for events with $M_W \geq 6.0$. Solutions are presented with lower hemisphere projection and dark quadrant denotes compression. The area of interest is enclosed by empty square. AG: Arabian Gulf; AS: Arabian Sea; BS: Bitlis Suture; CY: Cyprean Arc; DSF: Dead Sea Fault; GA: Gulf of Aden; IO: Indian Ocean; MS: Mediterranean Sea; RS: Red Sea; ZB: Zagros Belt. Dashed red, thin black and heavy blue lines represent the rifting, transform and subduction-collision boundaries, respectively. Ophiolite exposures are shown by violet colors.

Fig. 2. Local seismicity of UAE recoded by Dubai and Oman broadband stations from June 2006 to Feburary 2008. Blue lines are known surface faults crossing the area. Solid stars represent the gas filed in Dubai near Wadi Nazwa. MK: Makkran; ZFZ: Zenden Fault zone. Others symbols and seismicity data on the inset map are similar to Fig. 1.

Fig. 3. Topographic map of the studied area. Focal mechanisms of the studied earthquakes of March and September, 2007. The focal mechanism of March 2002 is also shown (Rodgers et al., 2005). Local seismicity recorded by Dubai and Oman networks from June 2006 to February 2008 is presented with symbols similar to Figure 2. Dashed line represents the suggested extension of the active NNE-SSW Bani Hamid fault.

Fig. 4. Focal mechanisms based on the polarities of P-wave of two studied earthquakes (A: 03/10/2007 & B: 13/09/2007). Lower hemisphere equal area projection is used.

Fig. 5. Comparison between observed (solid lines) and synthetic (dashed lines) displacement waveforms for the preferred focal mechanism deduced from the regional waveform inversion of 10/03/2007 main shock. The epicentral distance (km) and azimuth (degree) of each station is written above their trace. Z, R, T indicates vertical,

Radial and transverse components consequently. Time scale in sec and amplitude scale in μm are located to the bottom and left of the T component.

Fig. 6. Percent of variance reduction and source mechanism as a function of focal depths resulted from regional waveform inversion for 10/03/2007 main shock. Mechanisms are plotted each 2km only except the first 5km. Preferred solution is labeled above by its moment magnitude. Dark arrow indicates the preferred focal depth.

Fig. 7. Comparison between observed (solid lines) and synthetic (dashed lines) displacement waveforms for the preferred focal mechanism deduced from the regional waveform inversion of 13/09/2007 main shock. The epicentral distance (km) and azimuth (degree) of each station is written above their trace. Z, R, T indicates vertical, Radial and transverse components consequently. Time scale in sec and amplitude scale in μm are located to the bottom and left of the T component.

Fig.8. Percent of variance reduction and source mechanism as a function of focal depths resulted from regional waveform inversion for 13/09/2007 main shock. Mechanisms are plotted each 2km only and the preferred solution is labeled above by its moment magnitude. Dark arrow indicates the preferred focal depth.

Fig. 9. Displacement spectra from four selected stations for 10/03/2007 main shock. The station code, the distance in km and azimuth in degrees are given. Blue line indicates the spectrum while the red indicates the fitted omega-square source model curve.

Fig. 10. Displacement spectra from four selected stations for 13/09/2007 main shock. The station code, the distance in km and azimuth in degrees are given. Blue line indicates the spectrum while the red indicates the fitted omega-square source model curve.

Tables

Table 1: Hypocentral parameters of the two studied events.

Date			Origin Time			Location		H	Er. (km)			M_L	Ref
Day	Mo.	Yr.	H.	Mn.	Sec.	Lat.	Long.	(km)	X	Y	Z.		.
10	03	2007	18	15	14.3	25.303	56.191	4.2	04	03	05.0	4.0	*
					14.4	25.222	56.074	10f	6.6	5.7	-	4.1	**
13	09	2007	15	47	07.0	25.469	56.2972	8.2	03	2.2	04	4.4	
					08.7	25.460	56.200	20f	12.5	9.9	--	4.5	***

*, ** and ***: locations of this study, NEIC and CSEM, respectively. f: fix focal depth.

Table 2. Arabian Platform crustal model (Rodgers et al., 1999).

Thickness Km	**V_P Km/sec**	**V_S Km/sec**	**ρ gm/cm^3**
4	4.0	2.31	2.6
16	6.2	3.64	2.8
20	6.4	3.70	3.0
∞	8.1	4.55	3.2

Table 3. The focal mechanism and source parameters for March 10, 2007 and September 13, 2007 main shocks using polarities and regional waveform inversion.

Event index	**Fault plane**			**M_w**	**M_ox 10^{21} dyne.cm**	**H (km)**	**Method**
	St.°	**Dip°**	**Rake°**				
10 03 2007	41°	51°	-103°	--	--	06	POL
	37°	39°	-108°	3.66	3.79	06	INV
13 09 2007	25	65	-101	--	--	08	POL
	13	63	-115	3.94	9.98	08	INV

POL: focal mechanism using polarities method.
INV: focal mechanism and source parameters using regional waveform inversion.

Table 4. Source parameters of March 10, 2007 main shock deduced from P-wave spectra.

St. Code	Δ (km)	Az°	f_o (Hz)	Ω_o cm*s	M_o (dyne.cm)	r_o (m)	Δσ (bar)	d_o (cm)	Mw
BAN	69.70	9	2.72	4.41e-05	$4.00x10^{21}$	843	2.91	0.53	3.67
HAT	53.40	186	3.03	6.20e-05	$4.20\ x10^{21}$	755	4.13	0.70	3.68
ASH	70.10	191	2.94	4.13e-05	$3.85x10^{21}$	780	3.55	0.60	3.66
ASU	114.9	229	3.79	2.03e-05	$3.66\ x10^{21}$	604	7.25	0.95	3.64

Table 5. Source parameters of September 13, 2007 main shock deduced from P-wave spectra.

St. Code	Δ (km)	Az°	f_o (Hz)	Ω_o cm*s	M_o (dyne.cm)	r_o (m)	Δσ (bar)	d_o (cm)	Mw
BAN	50.50	0	3.60	1.75e-04	$13.4x10^{21}$	635	22.90	3.16	4.02
HAT	73.40	193	2.55	9.26e-05	$8.82\ x10^{21}$	896	5.36	1.04	3.90
ASH	90.50	195	2.29	4.83e-05	$5.73x10^{21}$	998	2.52	0.54	3.77
ASU	135.06	226.5	2.77	9.67e-05	$19.6\ x10^{21}$	826	15.22	2.73	4.13

Table 6. Mean value (M.V.), standard deviation (S.D.) and multiplicative error factors (M.E.) of the estimated seismic moment, M_o, the fault radius, r, the stress drop, Δσ, average displacement, d_o and moment magnitude, M_w.

	Main shock of March 10, 2007					***Main shock of September 13, 2007***				
	M_o (dyne.cm)	r_o (m)	Δσ (bar)	d_o (cm)	Mw	M_o (dyne.cm)	r_o (m)	Δσ (bar)	d_o (cm)	Mw
M. V.	$3.92\ x10^{21}$	739	4.19	0.67	3.67	$10.73\ x10^{21}$	827	8.28	1.48	3.95
S. D.	0.02	0.06	0.17	0.10	0.00	0.23	0.08	0.43	0.36	0.01
M. E	1.06	1.15	1.48	1.28	1.00	1.69	1.21	2.72	2.30	1.04